Volume 3
Number 1
1 January 2024
Pages 1–156

Sensors & Diagnostics

rsc.li/sensors

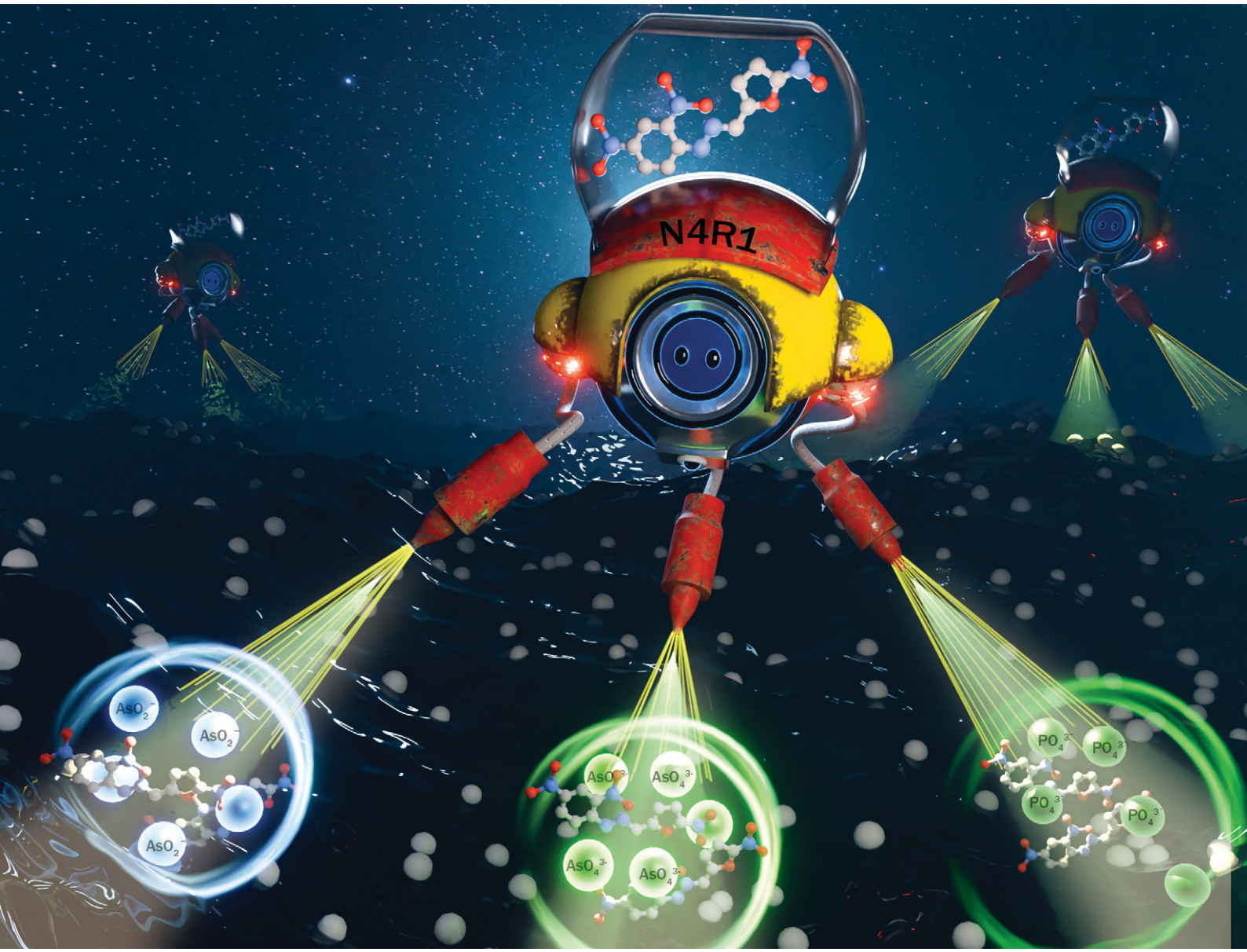

ISSN 2635-0998

ROYAL SOCIETY OF CHEMISTRY

PAPER

Darshak R. Trivedi *et al.*

Development of multi-analyte responsive sensors: optical discrimination of arsenite and arsenate ions, ratiometric detection of arsenite, and application in food and water samples

Sensors & Diagnostics

PAPER

View Article Online
View Journal | View Issue

Cite this: *Sens. Diagn.*, 2024, **3**, 64

Development of multi-analyte responsive sensors: optical discrimination of arsenite and arsenate ions, ratiometric detection of arsenite, and application in food and water samples†

Nagaraj K,[ab] A. Nityananda Shetty[a] and Darshak R. Trivedi *[b]

5-Nitro-2-furaldehyde based Schiff base chemosensors, N4R1–N4R3 with varying strengths of electron-withdrawing groups were developed for the discriminatory sensing of arsenite and arsenate ions in semi-aqueous media. Receptor N4R1 distinguished arsenite (AsO_2^-) and arsenate (AsO_4^{3-}) anions colorimetrically in 30% aq. acetonitrile (MeCN) with a detection limit of 18 ppb for arsenite. N4R1–N4R3 also detected phosphate, arsenite and arsenate in 30% aq. dimethyl sulfoxide (Me_2SO) solution and the selectivity for arsenite over arsenate was achieved at 50% aq. Me_2SO solution with a noticeable bathochromic shift near 200 nm. All three receptors exhibited ratiometric detection for arsenite and were identified as stable over the 6–12 pH range. The computed high binding constants of the receptors N4R1–N4R3 for inorganic arsenic anions and phosphate in the range of 10^6 M^{-1} exposed the receptor's higher potential in the sensing process. Hydrogen bonding interaction followed by deprotonation and the ICT mechanism on binding with arsenite/arsenate/phosphate was confirmed by UV-vis and ^{1}H-NMR titration, electrochemical studies, density functional theory studies, and mass spectral analysis. Fabrication of disposable paper strips and solid state sensing using silica gel were employed to conveniently detect arsenite and phosphate anions in real-life samples. The potential application of the receptors for detection in environmental and real-life samples was evaluated by analyzing food and water samples spiked with arsenite and phosphate anions.

Received 2nd August 2023,
Accepted 14th November 2023

DOI: 10.1039/d3sd00207a

rsc.li/sensors

1. Introduction

The development of colorimetric as well as fluorescent chemosensors has gained immense attention in the supramolecular research arena due to their improved selectivity and sensitivity.[1,2] The chemosensors were widely designed for the detection of various cations, anions, and small molecules.[1–8] The great need for developing optical sensors for ionic detection is also due to the increased pollution rates in the aquatic system by contamination by various ions. The traditional instrument-based detection process could not be sufficient for routine analysis of water samples. The sophisticated technology, high analysis cost, and requirement of expertise in handling restrict these methods from being used for regular water quality analysis.[9,10] Over the past few decades, colorimetric and fluorogenic sensing systems have emerged as an efficient alternative to the traditional instrument-based detection processes.[8–17] These techniques have the advantages of cost-effectiveness, simple synthesis, easy purification, and ease of operation. Many attempts have been made in recent years to sense various anions and cations using chromogenic and fluorogenic methods.[18–23] Most of these chemosensors were designed for monitoring the environment-polluting ions with precise detection and quantification.[20,24–30]

Among various environment-polluting ions, arsenic species are highly threatening to the ecological system and human health.[31] Groundwater pollution by arsenic compounds is a frequent concern due to their extreme toxicity. Accumulation of arsenic in the aquatic environment and soil is mainly due to anthropogenic actions like mining sulfide ores, industrial waste disposal, and improper use of pesticides and herbicides.[32] The arsenic contamination of aquatic systems eventually transfers these toxins to living systems, including humans, through the food chain. Between

[a] *Material Science Laboratory, Department of Chemistry, National Institute of Technology Karnataka (NITK) Surathkal, Srinivasnagar – 575 025, Karnataka, India*
[b] *Supramolecular Chemistry Laboratory, Department of Chemistry, National Institute of Technology Karnataka (NITK) Surathkal, Srinivasnagar – 575 025, Karnataka, India. E-mail: darshak_rtrivedi@yahoo.co.in, darshakrtrivedi@nitk.edu.in; Fax: +91 824 2474033; Tel: +91 824 2473205*
† Electronic supplementary information (ESI) available. See DOI: https://doi.org/10.1039/d3sd00207a

the two predominant forms of arsenic, inorganic ions are more toxic than organic arsenic species. Inorganic arsenic ions occur in two oxidation states, arsenite, As^{3+}, and arsenate, As^{5+}. Between these two inorganic arsenic anions, arsenite is considered to be more toxic due to its higher affinity towards thiol groups.[33] Excess exposure to arsenic and its accumulation in the human body can lead to cancer, skin diseases, cardiovascular diseases, and DNA damage. Hence, monitoring and removal of arsenic content in water and food samples are essential.[34,35]

Another anionic pollutant in water bodies is phosphate ions. Phosphate detection is vital due to its significance in biological, industrial, and agricultural uses.[36,37] Phosphates are a common component of fertilizers since the ion is an essential nutrient for plant growth. Phosphate enters water bodies through agricultural runoff which leads to eutrophication and depletion of oxygen, negatively impacting the aquatic ecosystems.[38] Excess consumption of phosphates causes various health issues, including bone health issues, kidney function impairment, cardiovascular diseases, and hormonal imbalances.[38]

Various colorimetric and fluorescent chemosensors were developed to detect arsenite (AsO_2^-), arsenate (AsO_4^{3-}), and phosphate (PO_4^{3-}) in organic and semi-aqueous media.[32,35,39–52] However, most of the detection strategies adopted fluorescence sensing. Colorimetric detection has the advantage of naked-eye visualization; hence, more efforts are needed to be made to design colorimetric sensors for inorganic arsenic anions. Also, the majority of the previous reports of arsenite/arsenate/phosphate sensors induce spectral absorption shifts of 50–100 nm.[40,49,53–56] The spectral shift towards higher wavelengths is important to make the color change more obvious and identify the anionic species immediately. Improving the water content of the receptor solution also requires more attention to make the receptors environment-friendly and appropriate for real-life applications. Also, it is noted from earlier studies on detecting arsenic species that no receptor has been created so that a single molecule sensor can identify both arsenite and arsenate with different color changes and different spectral shifts. The idea of multi-analyte sensors also gained visibility due to their cost-effectiveness compared to the single-analyte system and simultaneous measurement.

Analyzing these research gaps in recognition of arsenite/arsenate/phosphate ions, we have attempted to design multi-analyte colorimetric chemosensors for detecting both arsenic anions and phosphates in organo-aqueous media. Also, attempts were made to shift the absorption maxima towards the near-infrared region with a shift of 200 nm. Colorimetric differentiation of AsO_2^- and AsO_4^{3-} using a single receptor with observable color changes was also addressed. The objective of the current research work also focuses on the ratiometric detection of arsenite, which was less explored in the sensing process of arsenite by available previous research works.

Highlighting the above objectives and considering the limitations of the previously reported research works on the detection of inorganic arsenic anions and phosphates, we developed three receptors, N4R1–N4R3, based on 5-nitro-2-furaldehyde. All three Schiff base colorimetric sensors possess electron withdrawing groups of various strengths and an acidic binding site. Utilization of receptor N4R1 for the colorimetric differentiation of arsenite, arsenate, and phosphate in 30% aq. MeCN exhibits different color changes on binding with N4R1. All three receptors, N4R1–N4R3, were examined for their sensitive sensing properties for recognizing AsO_2^-, AsO_4^{3-}, and PO_4^{3-} in 30% aq. Me_2SO solution and discriminatory arsenite detection over the arsenate anion in 50% aq. Me_2SO solution. N4R1–N4R3 were also examined for the ratiometric detection of arsenite, and the stability of receptors and receptor–anion complexes in various pH ranges was studied. The detection mechanism was elucidated with the aid of UV-vis titration, ^{1}H-NMR titration, mass spectrometric analysis, cyclic voltammetric studies, and DFT studies. The real-life utility of the receptors was verified by constructing disposable paper strips, solid-state sensing using silica gel, and analyzing various food (vegetable and fruit juices) and water samples.

2. Experimental section

2.1. Materials and methods

The chemicals, solvents, and instruments used in the study are presented in the ESI.†

2.2. Synthesis of receptors (N4R1, N4R2 and N4R3)

The structure of the receptors N4R1–N4R3 is represented in Scheme 1. The synthetic procedure of the receptors is provided in the ESI.† Also, the structural characterization data and spectra of N4R1–N4R3 are included in the ESI† (Fig. S1–S12).

3. Results and discussion

3.1. Visual discrimination of arsenite, arsenate, and phosphate using N4R1

The colorimetric receptor N4R1 was employed for the detection of various anions in 30% aq. acetonitrile media. The preliminary studies to investigate the sensing properties of N4R1 (2×10^{-5} M, in 30% aq. MeCN) towards various sodium salts of anions (F^-, Cl^-, Br^-, I^-, AcO^-, NO_3^-, HSO_4^-, PO_4^{3-}, $H_2PO_4^-$, AsO_2^-, AsO_4^{3-}, SCN^-, $P_2O_7^{4-}$, S^{2-}, and N_3^-) were carried out by witnessing the color changes in N4R1 upon adding various anions. Receptor N4R1 was inactive towards all anions except phosphate, arsenite, and arsenate in 30% aq. MeCN (Fig. S13†). The addition of two equivalents of arsenite, arsenate, and phosphate anions to N4R1 brought a color change of yellow to blue for arsenite (AsO_2^-), yellow to pale green for arsenate (AsO_4^{3-}) and yellow to myrtle green for phosphate (PO_4^{3-}) (Fig. S14†). Hence, N4R1 can be used for the discriminatory recognition of AsO_2^- and AsO_4^{3-}, and the receptor could differentiate both inorganic anions with different colors, which are easily

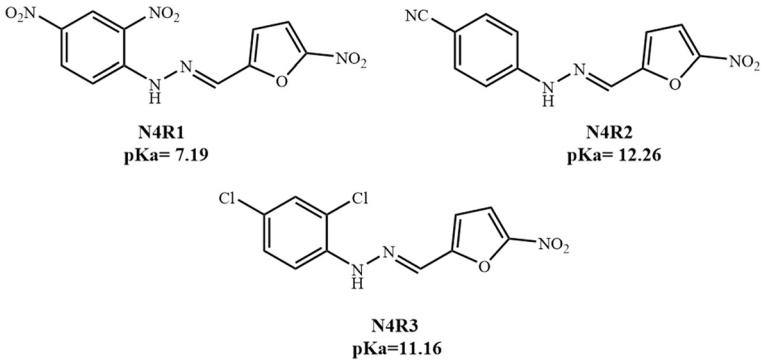

Scheme 1 Structure of receptors N4R1–N4R3 with pK_a values

distinguished. The receptor N4R1 in MeCN has also been checked for the detection of cations and was found to be inactive towards metal ions (Cu^{2+}, Hg^{2+}, Zn^{2+}, Ni^{2+}, Co^{2+}, Fe^{3+}, Pb^{2+}, Cd^{2+}, and Cr^{3+}) (Fig. S15†).

The binding characteristics of N4R1 with arsenite, arsenate and phosphate ions were further examined with UV-vis titration experiments in 30% aq. MeCN solution. The titration experiments supported the visual distinction of phosphate, arsenite and arsenate with considerable spectral shift differences. An absorption band characterizes the receptor N4R1 at 418 nm, which corresponds to the π–π* transition.[57] The sequential addition of AsO_2^- (1×10^{-2} M, in H_2O) caused a gradual decrease in the absorption intensity of the band at 418 nm, and a new band emerged at 595 nm. An isosbestic point at 467 nm established the development of single species in the specific binding ratio (Fig. 1a). Addition of AsO_2^- to N4R1 altered the initial yellow color of N4R1 to blue with spectral shifts. Similarly, the addition of the arsenate anion caused the emergence of a new band at 601 nm with an isosbestic point of 460 nm. The arsenate anion suppressed the absorption intensity at 418 nm, and the bathochromic shift induced a yellow to green color change in the receptor solution (Fig. 1b). The phosphate addition induced a new band at 592 nm with an isosbestic point of 469 nm (Fig. 1c).

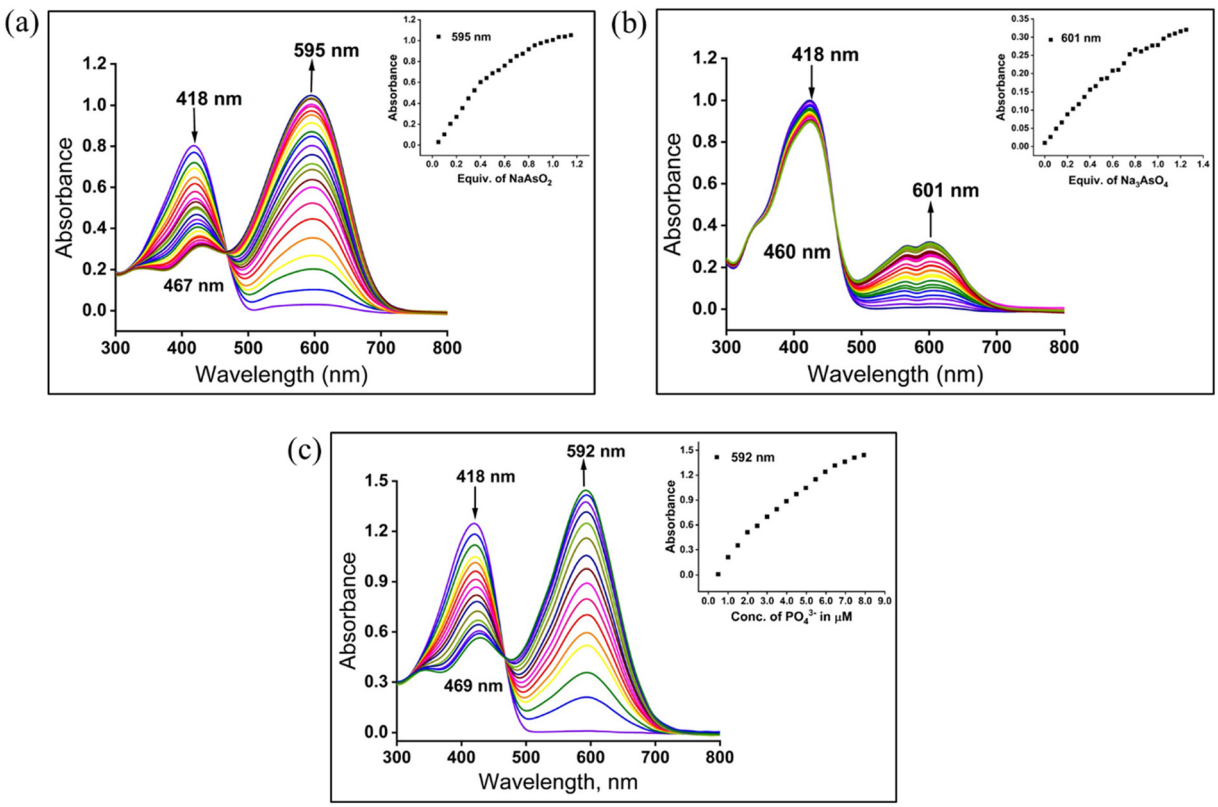

Fig. 1 The absorption variations of N4R1 (2×10^{-5} M in 30% aq. MeCN) with stepwise addition of (a) $NaAsO_2$, (b) Na_3AsO_4 and (c) Na_3PO_4 (1×10^{-2} M in H_2O). Inset plots signify absorption changes with anion addition.

UV-vis titration experiments showed that the binding of arsenite, arsenate and phosphate ions caused different spectral shifts to the receptor N4R1. Arsenite addition induced a bathochromic shift of 177 nm, arsenate addition caused a shift of 183 nm and phosphate addition induced a redshift of 174 nm. These dissimilar spectral shifts by arsenite, arsenate, and phosphate introduced different color changes to the N4R1 system. Hence, receptor N4R1 in 30% aq. MeCN can be used as an effective colorimetric sensor to differentiate inorganic arsenic anions of different oxidation states.[58] N4R1 also differentiated phosphate from arsenite and arsenite with a dissimilar color even though the ion has minimal difference from the λ_{max} of arsenite.

The receptor N4R1 in 30% aq. MeCN medium also detects arsenite in a ratiometric manner with diverse color changes for different equivalents of arsenite. The yellow color of the receptor N4R1 changed to pale green, dark green, peacock blue, and violet-blue on the addition of 0.5–2.0 equivalents of arsenite with stepwise addition of 0.5 equivalents (Fig. 2). The variation in the absorption maxima intensity, as well as the color change, is due to the initial hydrogen bonding interaction of arsenite with the binding site and the deprotonation process in the higher concentrations of arsenite. The ratiometric color changes were observable up to the concentration of 1×10^{-5} M in water as shown in Fig. S16.†

3.2. Aqueous tolerance study

Application of sensors for examining real-life and natural samples requires the detection process in semi-aqueous or pure aqueous media. The sensor's aquatic content can alter the receptor binding site's H-bonding capacity. Hydration of the anion can also affect the ion's basicity, thereby influencing the binding strength and nature. The aqueous tolerance of arsenite, arsenate, and phosphate anions was studied by changing the water fraction in the receptor solution. In the semi-aqueous system of Me_2SO–H_2O with 30% water content, receptors N4R1–N4R3 displayed selectivity towards AsO_2^-, AsO_4^{3-}, and PO_4^{3-} anions. Further increment in the water content to 50% in the receptor solutions caused the selective recognition of the AsO_2^- anion over the AsO_4^{3-} anion. In 50% aq. Me_2SO solution, AsO_4^{3-} could not report any coloration, whereas the AsO_2^- anion was able to retain its binding characteristics. Meanwhile PO_4^{3-} ions could exhibit color up to 50% water content, even though a decrease in the absorption intensity was observed. The sensing ability of receptors towards arsenite and phosphate anions vanished when the water content increased beyond 50% (Fig. 3 and S17†). These observations can be described using the solvation energy of arsenite and arsenate and their basicity. Between the two inorganic arsenic anions, arsenate possesses a higher charge density than arsenite. Because of the high charge density of AsO_4^{3-}, the extent of hydration will be higher for AsO_4^{3-} than AsO_2^-. The extent of hydration decreases the anion's basicity and weakens binding with the receptor.[59] Both inorganic arsenic anions and phosphate can maintain their basicity and binding strength to 30% of water content. Hence, the detection process of arsenite, arsenate, and phosphate was performed in 30% aq. Me_2SO. Although AsO_2^- has a lower hydration energy than AsO_4^{3-}, it can maintain its basicity and binding characteristics until the water concentration reaches 50%. Thus, the discriminating detection of AsO_2^- over AsO_4^{3-} was done at 50% aq. Me_2SO solution.

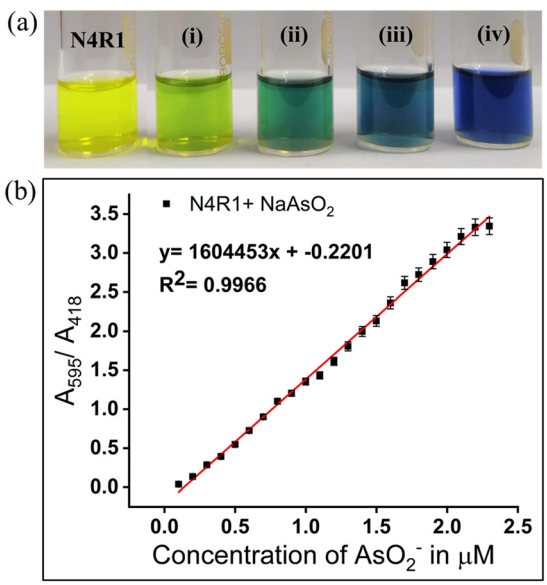

Fig. 2 (a) Ratiometric color change of N4R1 (2×10^{-5} M, 30% aq. MeCN) on addition of (i) 0.5 equivalents, (ii) 1 equivalent, (iii) 1.5 equivalents and (iv) 2 equivalents of $NaAsO_2$ (1×10^{-2} M, in H_2O). (b) Ratiometric plot of A_{595}/A_{418} for N4R1 with the cumulative addition of the AsO_2^- ion.

3.3. Detection of arsenite, arsenate, and phosphate in 30% aq. Me_2SO

Receptors N4R1–N4R3 exhibited sensing ability towards AsO_2^-, AsO_4^{3-} and PO_4^{3-} in 30% aq. Me_2SO solution.

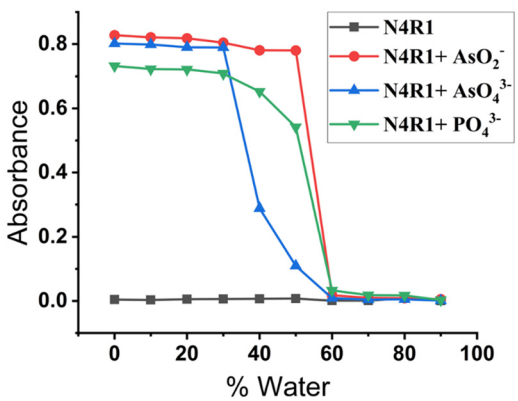

Fig. 3 UV-vis spectral response of N4R1 and N4R1 + AsO_2^-/AsO_4^{3-}/PO_4^{3-} in different water contents in Me_2SO.

Visual inspection of color changes induced by AsO_2^-, AsO_4^{3-}, and PO_4^{3-}, in semi-aqueous media (2×10^{-5} M, 30% aq. Me_2SO) by adding two equivalents is presented in Fig. S19.† The yellow color of receptor N4R1 changed to blue on adding two equivalents of AsO_2^-, AsO_4^{3-}, and PO_4^{3-}. Similarly, N4R2 changed from yellow to green, and N4R3's color changed to peacock green with the addition of arsenite, arsenate and phosphate, as shown in Fig. S19.† Other anions (F^-, Cl^-, Br^-, I^-, AcO^-, NO_3^-, HSO_4^-, $H_2PO_4^-$, SCN^-, $P_2O_7^{4-}$, S_2^-, and N_3^-) were unable to alter the receptors' color in 30% aq. Me_2SO solution. Binding experiments with UV-vis absorption spectroscopy confirmed the observations. Detection of metal ions using N4R1–N4R3 in 30% aq. Me_2SO was carried out using 1×10^{-2} M water solutions of various metal ions. However the metal ions did not impart any color changes to the receptor solutions (Fig. S19†).

UV-vis titration experiments were performed in 30% aq. Me_2SO solution to understand the binding affinity of receptors N4R1–N4R3 towards AsO_2^-, AsO_4^{3-}, and PO_4^{3-}. On steady addition of AsO_2^- and AsO_4^{3-}, the absorption band at 440 nm of N4R1 diminished, and a new red-shifted band appeared with $\Delta\lambda_{max}$ of 178 nm at 618 nm for arsenite and $\Delta\lambda_{max}$ of 179 nm at 619 nm for arsenate. An isosbestic point of 482 nm and 483 nm was observed for AsO_2^- and AsO_4^{3-}, respectively (Fig. S20 and S21†). Similarly, the sequential addition of PO_4^{3-} caused a new bathochromic shifted absorption band at 591 nm with an isosbestic point of 480 nm (Fig. S22†). The –NH moiety in N4R1 acts as the binding site for the inorganic arsenic anions and phosphate ions. The existence of two electron-withdrawing nitro groups makes the binding site more acidic, thereby facilitating an effective hydrogen bonding interaction with arsenite/arsenate/phosphate. The further addition of the anion deprotonates the –NH proton, leaving the N– group in N4R1. The electron-rich –NH moiety interacts with the electron-deficient nitro groups *via* intramolecular charge transfer (ICT). The process induces a spectral shift in the receptor and color change.

Receptor N4R2, with an absorption band centered at 448 nm, changes its color to green by adding AsO_2^-, AsO_4^{3-}, and PO_4^{3-}. The stepwise addition of AsO_2^-, AsO_4^{3-}, and PO_4^{3-} caused a red shift in the spectra towards 675 nm for arsenite, 674 nm for arsenate and 656 nm for phosphate. Isosbestic points at 514 nm, 511 nm, and 523 nm, respectively, for arsenite, arsenate, and phosphate indicate the strong complex formation between N4R2 and the studied anions (Fig. S23–S25†). The electron-withdrawing cyanide group acts as the signaling unit, making the –NH proton more acidic. Initial hydrogen bonding interaction of –NH and arsenite/arsenate/phosphate followed by deprotonation facilitates the ICT mechanism.

In 30% aq. Me_2SO solution, receptor N4R3 changes color from yellow to peacock green upon the addition of arsenite, arsenate, and phosphate. The absorption band at 446 nm of the free N4R3 observed a decrease in intensity on stepwise addition of arsenite, arsenate, and phosphate, and a bathochromically shifted new absorption band emerged at 668 nm for all three ions (Fig. S26–S28†). The spectral shift of 222 nm is responsible for the color change. The ICT mechanism in the receptor–anion complex was observed between the electron-withdrawing –Cl groups and the electron donating –NH moiety.

All three receptors N4R1–N4R3 contain electron-withdrawing groups of varying strengths. These electron-withdrawing groups act as signaling units and enhance the acidic nature of the –NH binding site. Hence, the strength of electron-withdrawing groups in the receptors affects the detection process. N4R1 contains two $-NO_2$ groups, N4R2 contains one –CN group, and N4R3 has two –Cl groups in its structure. The electron withdrawing strength follows the following order $-NO_2 > -CN > -Cl$. Meanwhile the presence of two –Cl in N4R3 makes –NH more acidic than that of one –CN group in N4R2. It is also evident from the pK_a values of N4R2 and N4R3. As the acidity of the binding site increases, it facilitates effective binding with basic anionic species. Hence, N4R1 binds with anions more efficiently than N4R2 and N4R3. Between N4R2 and N4R3, N4R3 has higher binding capacity compared to N4R2.

3.4. Selective detection of arsenite over arsenate anion in 50% aq. Me_2SO

N4R1–N4R3, which were active for both AsO_2^- and AsO_4^{3-} in 30% aq. Me_2SO solutions, were modified by changing the water content to attain specific selectivity for the arsenite anion over arsenate. Extending the water content to 50% in the receptor in Me_2SO selectively detected arsenite, whereas arsenate anions failed to impart any color to the system with 50% water content. Arsenite (As^{3+}) has lower charge and larger size compared to arsenate (As^{5+}) and contains lower charge density. Hydration of the arsenate anion is higher than arsenite due to the high charge density of AsO_4^{3-}. At 50% water content, the arsenate anion's basicity is affected, and its ability to attach to receptors is weakened. Due to this, the receptor becomes inactive towards colorimetric sensing of arsenate. In contrast, the arsenite anion could maintain its basicity and binding properties at 50% aq. Me_2SO due to its lower hydration energy.

UV-vis titration experiments were executed to analyze the binding characteristics of receptors N4R1–N4R3 in 50% aq. Me_2SO solution. Receptor N4R1 showed a red-shifted new band at 618 nm with an isosbestic point of 482 nm on gradually adding arsenite (Fig. 4). N4R2, with a distinctive absorption band at 448 nm, observed a decrease in the absorption intensity with a new red-shifted band at 675 nm on sequential addition of arsenite, as presented in Fig. S29.† A comparable trend was detected for receptor N4R3 with the emergence of a new band at 673 nm and an isosbestic point of 508 nm (Fig. S30†). All three receptors N4R1–N4R3 contain comparatively strong electron-withdrawing groups and a binding site of the acidic –NH moiety. The initial complexation with the basic arsenite anion to the –NH moiety is due to the weak hydrogen bonding interaction.

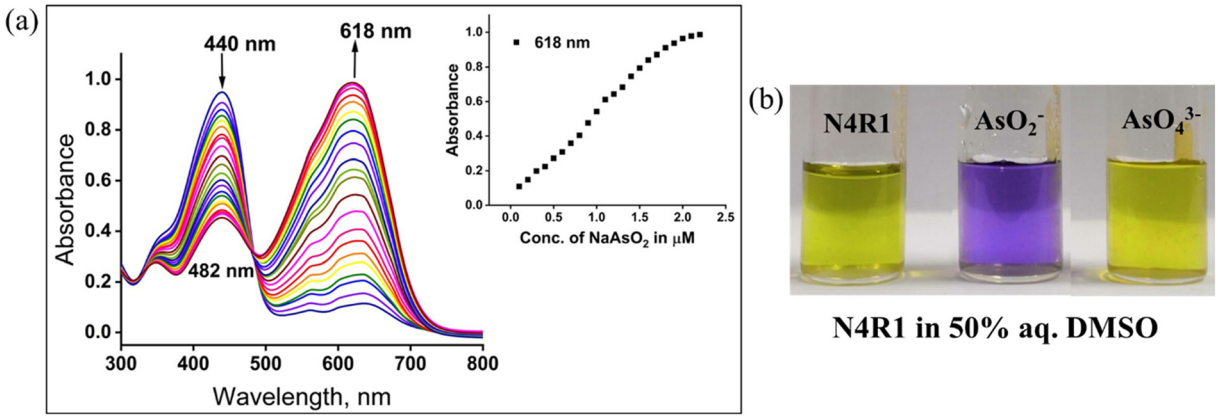

Fig. 4 (a) The absorption variations of the receptor N4R1 (2×10^{-5} M in Me_2SO–H_2O, 1 : 1 v/v) with sequential addition $NaAsO_2$ (1×10^{-2} M in water); inset plot represents absorption variations with arsenite addition. (b) color change of N4R1 (2×10^{-5} M, 50% aq. Me_2SO) on adding 2 equiv. of anions.

Excess addition of the arsenite abstracts the proton from the –NH moiety, which produces an ICT mechanism within the molecule between the electron-rich binding site and the electron-deficient signaling units. The process eventually results in spectral changes along with observable color changes. The absorption spectral data of receptors are tabulated in Table S1.†

3.5. Effect of the co-existence of other ions – interference study

The effect of the co-existence of other anions on the detection of AsO_2^-, AsO_4^{3-}, and PO_4^{3-} anions is examined using interference studies. Three equivalents of anions were added to the receptor–anion solution. The absorption band changes and the absorption band intensity variations were noted to

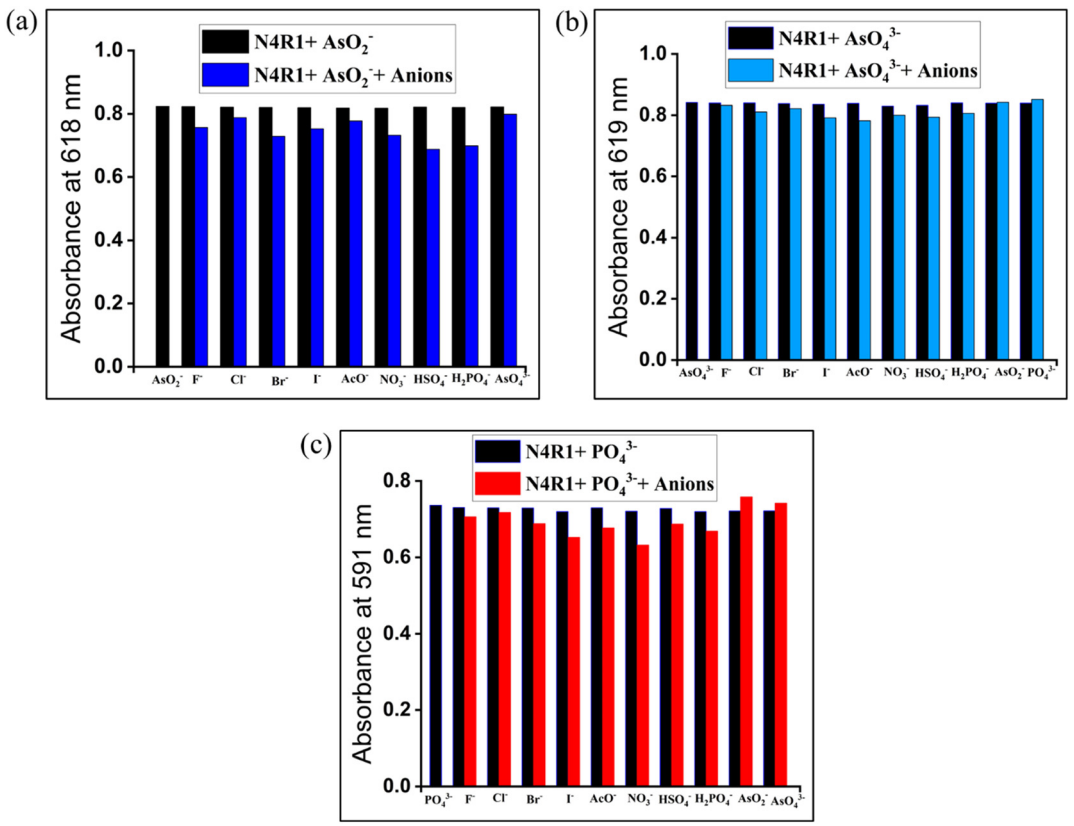

Fig. 5 Outcome of competing anions in the occurrence of 3 equiv. of different anions in the (a) 30% aq. Me_2SO solution (2×10^{-5} M), black bar: N4R1 + AsO_2^- ion, blue bar: N4R1 + AsO_2^- + competing anions, (b) 30% aq. Me_2SO solution (2×10^{-5} M), black bar: N4R1 + AsO_4^{3-} ion, sky blue bar: N4R1 + AsO_4^{3-} + competing anions, and (c) 30% aq. Me_2SO solution (2×10^{-5} M), black bar: N4R1 + PO_4^{3-} ion, red bar: N4R1 + PO_4^{3-} + competing anions.

identify the interferences. For interference studies, 30% aq. Me_2SO solutions were used, and the variation in the absorption intensity was plotted as a bar diagram in Fig. 5 and S31–S33.† The studies showed that the other anions did not cause any interference in the selective detection of AsO_2^-, AsO_4^{3-}, and PO_4^{3-}. Interference of various metal ions was also studied in the same procedure for arsenite, and the variation in absorption intensities was plotted (Fig. S34 and S35†). The presence of metal ions has the least interference in the detection of arsenite.

3.6. pH study

The stability of free N4R1–N4R3 and their AsO_2^-/AsO_4^{3-}/PO_4^{3-} complexes in acidic and basic media was evaluated using 0.05 M HEPES buffer solution. The UV-vis absorption profiles of N4R1–N4R3 and anion–bound receptors were analyzed over a pH range of 1–12. All three receptors were stable over the pH range of 1–9 and did not induce any notable variations in the UV-vis absorption intensity. This shows that N4R1–N4R3 are stable in acidic media. Meanwhile in higher basic media (pH > 9), acidic hydrogens in the free receptor undergo deprotonation, resulting in a considerable absorption intensity increase. The anion-bound receptors could not induce absorption spectral changes until pH 6. This is probably because of the feeble complexing capacity of AsO_2^-/AsO_4^{3-}/PO_4^{3-} ions due to their low stability in the acidic pH range. Receptor–anion species were discovered to be stable from pH 6 to 12, with a consistent absorbance intensity (Fig. 6 and S36–S40†).

3.7. Ratiometric detection of the arsenite anion

N4R1–N4R3 exhibited ratiometric recognition of the AsO_2^- ion with step-by-step addition of the anion. Receptor N4R1 has yellow color in 30% aq. Me_2SO solution and the color of the receptor changed to pale green with the addition of 0.5 equivalents of arsenite anion. One equivalent of arsenite addition changed the N4R1 color to dark green, and 1.5 and 2.0 equivalents of arsenite induced the color of blue and violet-blue, respectively (Fig. S41a†). The ratiometric detection of the arsenite anion also helps to quantify the amount of arsenite present in the sample with color changes. The possible reason for the ratiometric color changes could be the variation in the absorption maxima intensity with various concentrations of arsenite. The A_{618}/A_{440} ratio and the concentration of AsO_2^- ion to N4R1 had a good linear relationship, allowing the receptor to function as an absorption ratiometric chemosensor for quantitatively recognizing the arsenite anion (Fig. S41b†). Smaller concentrations of arsenite cause the hydrogen-bonding interaction with the receptor binding site. The hydrogen bonding interaction becomes more prominent on increasing the arsenite concentrations, and the basic arsenite anion could abstract the hydrogen from the binding site. The deprotonation process facilitates the ICT mechanism, and the intensity of the absorption band increases; these processes are reflected in the color changes in the receptor solution. Similarly, for receptor N4R2, the stepwise addition of arsenite with 0.5 equivalents changes the receptor color from yellow to straw yellow, pale green, dark green, and cyan. The ratiometric detection of arsenite using N4R2 and N4R3 in Me_2SO also followed the same patterns of color changes as shown in Fig. S42 and S43.†

3.8. Determination of the binding ratio, binding constant, and detection limit

The Benesi–Hildebrand (B–H) plot and the B–H equations using UV-vis titrations were used to determine the binding ratio and the binding constant of N4R1–N4R3 with AsO_2^-, AsO_4^{3-}, and PO_4^{3-} anions.[60,61] The linearity of the B–H plot on the first power of anion concentration confirmed the 1 : 1 binding between the receptors and arsenite/arsenate/phosphate (Fig. S44–S50†). The calibration curve between the anion concentration and the receptor–anion complex absorbance was utilized to calculate the limit of detection (LOD) (Fig. S51–S57†). The binding ratio, binding constant, and LOD of receptors N4R1–N4R3 are tabulated in Table 1 and Table S2.†

3.9. Cyclic voltammetric studies

The electrochemical properties of the receptors N4R1–N4R3 and the changes in the electrochemical properties with

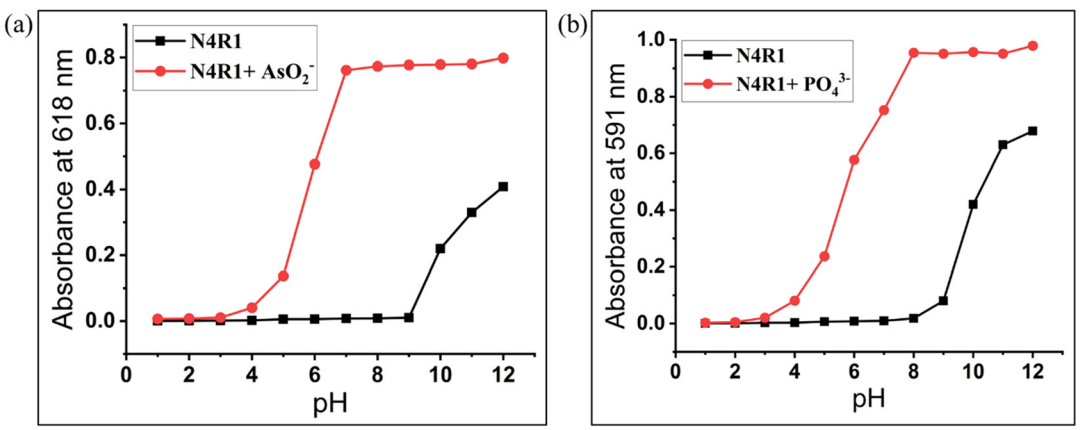

Fig. 6 pH effect on the UV-vis absorption spectra of (a) N4R1 and N4R1 + AsO_2^- and (b) N4R1 and N4R1 + PO_4^{3-} in Me_2SO–H_2O (7 : 3, v/v).

Table 1 Binding ratio, binding constant, and detection limit of receptors N4R1 in the presence of arsenite, arsenate, and phosphate ions

Receptor + anion	Solvent	Binding ratio	Binding constant (M^{-1})	Detection limit (ppb)
N4R1 + $NaAsO_2$	30% aq. MeCN	1 : 1	4.846×10^5	18.05
N4R1 + Na_3AsO_4	30% aq. MeCN	1 : 1	6.446×10^5	39.24
N4R1 + Na_3PO_4	30% aq. MeCN	1 : 1	3.543×10^5	132.19
N4R1 + $NaAsO_2$	30% aq. Me_2SO	1 : 1	4.060×10^5	43.97
N4R1 + $NaAsO_2$	50% aq. Me_2SO	1 : 1	2.765×10^6	39.58
N4R1 + Na_3AsO_4	30% aq. Me_2SO	1 : 1	5.765×10^5	43.96
N4R1 + Na_3PO_4	30% aq. Me_2SO	1 : 1	9.840×10^4	152.53

arsenite/arsenate/phosphate complexation were studied using cyclic voltammetric studies. A three electrode cell comprising a calomel electrode as the reference, platinum wire as the counter, and platinized platinum electrode as the working electrode was used for the studies in Me_2SO media. Tetrabutylammonium perchlorate was used as the supporting electrolyte. The cyclic voltammogram of free receptors N4R1, N4R2, and N4R3 exhibited anodic peaks at 0.65 V, 0.62 V, and 0.69 V, respectively, matching the –NH oxidation.[62] On regular addition of AsO_2^- anion, the intensity of the oxidation peak increases with a slight shift of the oxidation peak to 0.73 V, 0.74 V, and 0.76 V for the arsenite complex of N4R1–N4R3, respectively. The cathodic peak observed for the receptors N4R1–N4R3 was found to be −1.06 V, −1.01 V, and −1.05 V, respectively. The reduction peak intensity increased slightly towards −1.01 V, −0.98 V, and −0.99 V, respectively, for N4R1–N4R3 on successive addition of arsenite anion (Fig. 7a and S58†). Addition of phosphate ion intensified the oxidation peak with a slight shift towards 0.68 V, 0.87 V, and 0.77 V and reduction peak towards −0.92 V, −0.93 V and −1.04 V, respectively, for N4R1, N4R2, and N4R3 (Fig. 7b and S59†). A similar trend was observed on the addition of arsenate ion to the receptors (Fig. S60 and S61†). The shifts in the oxidation and reduction peaks imply the electron density increase over the receptor–anion complex due to strong H-bonding between the NH proton in the receptor and AsO_2^-/AsO_4^{3-}/PO_4^{3-}. Along with UV-vis titration experiments, cyclic voltammetric studies support the hydrogen bonding interaction between the receptor and anions.

3.10. ^{1}H-NMR titration

^{1}H-NMR titrations were carried out in Me_2SO-d_6 solvent to understand the sensing mechanism of receptors N4R1–N4R3 for arsenite anions. The receptor N4R1 is characterized with a ^{1}H-NMR peak at 11.91 ppm, which corresponds to the –NH proton. This –NH moiety acts as the binding site for AsO_2^-. On step-wise addition of arsenite, it was observed that the intensity of the peak at 11.91 ppm gradually decreased. This can be attributed to the strong hydrogen bonding interaction between the arsenite and the –NH proton. With an addition of 1 equivalent of arsenite anion, the peak corresponding to the –NH proton diminished, proving that the excess concentration of arsenite could abstract or deprotonate the –NH proton (Fig. 8). Similar observations were repeated for N4R2 and N4R3 (Fig. S62 and S63†). The intensity of the –NH peak at 11.51 in N4R2 and 10.75 in N4R3 decreased on steady addition of AsO_2^- ion, and the peak entirely vanished on adding 1 equivalent of AsO_2^- ion. These observations strongly support the initial H-bonding interaction followed by a deprotonation mechanism for detecting AsO_2^- using receptors N4R1–N4R3. A blank ^{1}H-NMR titration experiment was conducted with N4R1 and N4R2 in the absence of arsenite ions, using only water (H_2O) (Fig. S64 and S65†). No changes were observed in the peaks of ^{1}H-NMR spectra of the receptors, confirming that the deprotonation of the NH proton is a result of the interaction with arsenite, and not due to proton exchange with water.

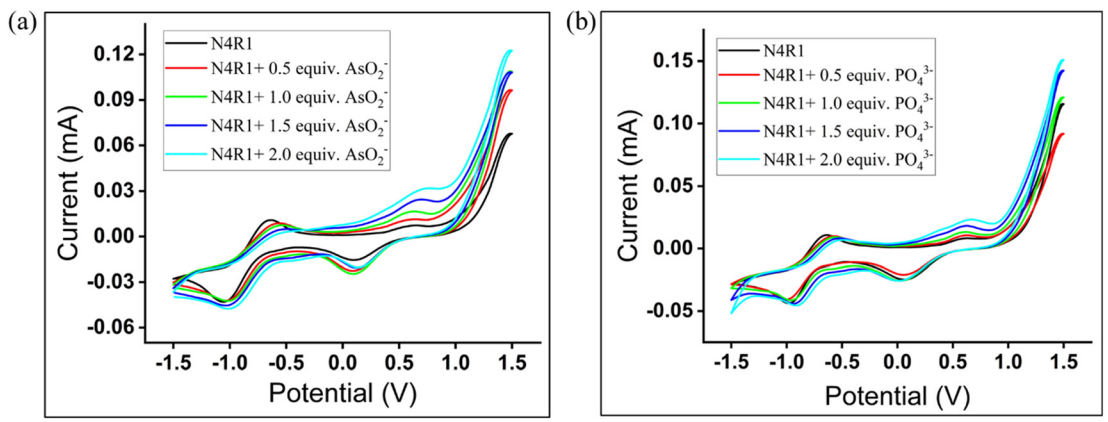

Fig. 7 CV diagram of N4R1with the sequential addition of (a) AsO_2^- and (b) PO_4^{3-} ions.

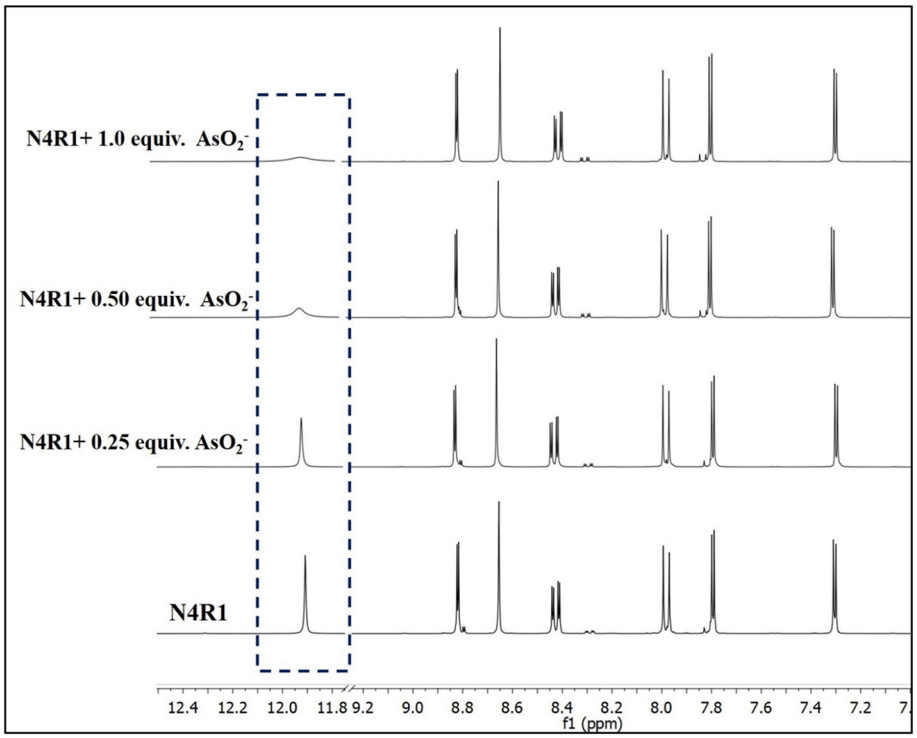

Fig. 8 ^{1}H NMR titration of N4R1 in a Me_2SO-d_6 solvent with sequential addition of (0–1 equiv.) of $NaAsO_2$ (1×10^{-2} M in H_2O).

3.11. Anion binding studies by mass spectrometry

Evidence for the mechanism of sensing was strengthened using mass spectral analysis. The mass spectra of the receptor–anion complex were noted and confirmed the binding mechanism and stoichiometric ratio of the binding. The LC-MS mass spectrum of the N4R1–arsenite complex indicated a peak at *m*/*z*: 449.9135 and *m*/*z*: 426.9097 which corresponds to the $[N4R1 + NaAsO_2]$–H^+ and $[N4R1 + AsO_2^-]$–H^+ respectively. The mass spectrum of the N4R1–arsenate complex indicated peaks for $[N4R1 + AsO_4^{3-}]$–H^+ and $[N4R1 + Na_3AsO_4]$–H^+ with *m*/*z*: 458.9175 and *m*/*z*: 527.9142. Similarly, N4R2–arsenite and N4R2–arsenate complexes showed a spectral peak at *m*/*z*: 362.1161 and *m*/*z*: 394.2165, respectively. All the values match with the calculated *m*/*z* values. Mass spectral data of the receptor–anion complexes confirm the 1 : 1 binding between the receptor and the arsenite/arsenate, and support the deprotonation mechanism. The ESI† presents the corresponding LC-MS spectra in Fig. S66–S69.

3.12. DFT studies

Theoretical calculations were carried out using the Turbomole V7.5 software package to validate and support the experimental observations of arsenite sensing by N4R1–N4R3. The density functional theory (DFT) approach was employed to optimize the geometries of free receptors and the receptor–arsenite complex. The geometry optimization used software-generated C_1 point group symmetry with the B3LYP functional and def-TZVPP basis set.[63] The receptor's and complex's excited state properties were determined using the time-dependent DFT (TD-DFT) method with the same basic set and functional. The electron density distribution in the HOMO and LUMO of the free receptor and the arsenite-bound receptors is shown in Fig. 9, S70 and S71.† There was a significant reduction in the band gap energy of the arsenite–bound receptors compared with the band gap energy of free receptors. This lowering of the band gap is accountable for the red shift in the absorption spectra on complexation with arsenite and the resultant color changes.

The HOMO–LUMO gap computed for receptor N4R2 is 2.765 eV. Binding of AsO_2^- with N4R2 decreased the band gap to 1.976 eV (Fig. 9). This lowering of the band gap is supported by the spectral shift of 227 nm in the UV-vis absorption spectra. The differences in the electron density distribution in the HOMO and LUMO of N4R2 and the N4R2–arsenite complex confirmed the possible charge transfer process. The LUMO of N4R2 is confined in the nitro group connected to the thiophene ring, and the electron density in the HOMO is distributed over the NH moiety. On complexation with arsenite, HOMO, and LUMO, molecular orbitals are stabilized by a decrease in energy that results in the shortening of the band gap. The LUMO of the N4R2–arsenite complex is distributed over the –NH group and the nitro group, and the electron density in HOMO is localized in the NH group. The MO diagrams also reveal that the acidic –NH hydrogen of N4R2 is deprotonated by the basic AsO_2^- ion. And there is a weak H-bonding interaction between the binding site and the arsenite.

Similarly, the electron density of the LUMO and HOMO of free N4R3 is distributed in the nitro group and –NH moiety,

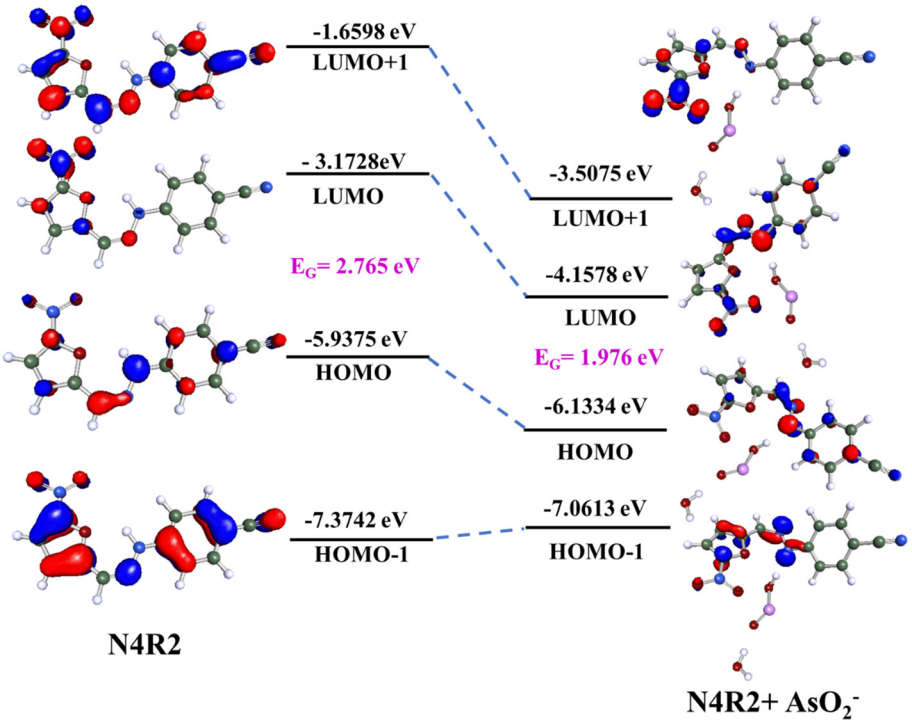

Fig. 9 HOMO and LUMO diagrams for N4R2 and N4R2–AsO_2^- by the B3LYP/def-TZVPP method.

respectively, and the complexation stabilizes the lowest unoccupied molecular orbital resulting in a reduction in the band gap from 2.667 eV to 1.943 eV (Fig. S70†). The reduction in HOMO–LUMO gap is responsible for the spectral shift of 222 nm in the case of N4R3 on complexation with AsO_2^-. The receptor N4R1 also followed a similar trend and is presented in Fig. S71.† The excited state characteristics of free receptors and the complex are evaluated using TD-DFT calculations (Table S3†). The absorption maxima calculated using TD-DFT for the receptor and the receptor–AsO_2^- complexes are comparable with the absorption maxima obtained using UV-vis spectroscopy (Fig. 10 and S72†). In Fig. 10a, the absorption band at 496 nm decreases in the presence of arsenite anion, and a new band emerges at 663 nm. A similar trend was observed in the experimental UV-vis titration experiment. The 496 nm absorption band corresponds to the characteristic band of N4R2; on complexation with arsenite, hydrogen bonding interaction occurs between N4R2 and the arsenite anion. The process is confirmed by the decrease in the intensity of the band at 496 nm and formation of a new band at 663 nm, confirming the presence of a new species in the system. A comparison of the experimental and theoretically calculated absorption shifts is presented in Table S4.†

3.13. Reversibility study

Reversibility studies were conducted on the receptor–anion complex with Ca^{2+} ions. A specified amount of Ca^{2+} (in the

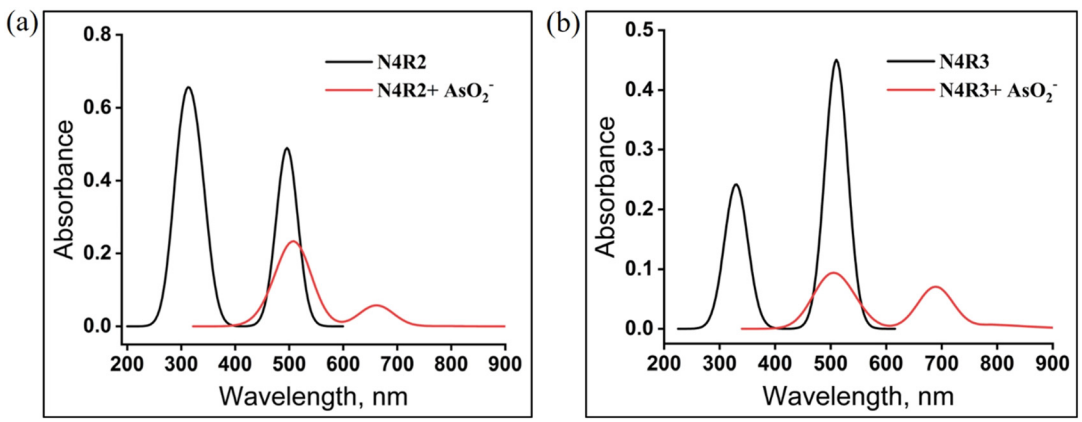

Fig. 10 UV-vis absorption spectra of a) N4R2 and b) N4R3 and AsO_2^- ion complexes calculated by the TD-DFT method.

form of Ca $(NO_3)_2$, 1×10^{-2} M in H_2O) was added to receptor–anion solution (2×10^{-5} M in 30% aq. Me_2SO), and observations were made regarding the changes in color as well as the UV-vis absorption intensity. In the case of all three receptors N4R1–N4R3, arsenate and phosphate exhibited superior recyclability upon the addition of 40 μL of Ca^{2+} for N4R1, and 20 μL for both N4R2 and N4R3. The receptor–arsenate/phosphate complex changed its color instantaneously upon the addition of Ca^{2+} ions, with a restoration of the initial absorption characteristics of the free receptor (Fig. S73†). This reversibility was sustained for up to 5 cycles, indicating a strong interaction between Ca^{2+} and arsenate/phosphate, highlighting the system's high quality (Fig. S74†).

On the other hand, in the case of arsenite (AsO_2^-), the color and spectral characteristics of the receptor–arsenite complex were maintained up to the addition of 100 μL for N4R2 and N4R3–arsenite complexes, and 300 μL for the N4R1–arsenite complex (Fig. S75 and S76†). This is attributed to the weaker interaction and lower reactivity between arsenite and calcium ions. Based on this experiment, it can be concluded that arsenite can be selectively distinguished from arsenate and phosphate with a reversibility study using Ca^{2+} ions. While arsenate and phosphate display reversibility in the presence of Ca^{2+}, arsenite does not exhibit similar changes.

3.14. Possible detection mechanism

The recognition mechanism of AsO_2^- using N4R1–N4R3 has been proposed using UV-vis titration, ^{1}H-NMR titration, cyclic voltammetric studies, mass spectral analysis, and DFT studies. The receptors N4R1–N4R3 contain an acidic binding site –NH and the electron-withdrawing groups in their structure. On addition of the basic arsenite anion, initially, there will be H-bonding interaction between the arsenite and the –NH. The excess arsenite ion deprotonates the –NH proton, leaving the N– group in the receptor. The electron-withdrawing groups in the receptor structure act as the electron-deficient moiety, and the binding site –NH, acts as the electron-rich center to enable the intramolecular charge transfer (ICT) mechanism supported by the arsenite ion binding. This process is responsible for the spectral shift in the UV-vis spectra and the color change of the system. The possible binding mechanism of N4R1 with the arsenite anion is shown in Scheme 2.

3.15. Analytical applications

3.15.1. Fabrication of test strips. Chromogenic test strips were developed using receptors N4R1–N4R3 for the on-site recognition of arsenite and phosphate. Whatman filter papers were cut into rectangular shapes and soaked in the receptor solution in 30% aq. Me_2SO and dried in the oven. The receptor-coated test strips were used to detect arsenite and phosphate in various samples. The pale yellow color test trip of N4R1 turned pale blue on adding 0.5 equivalents of AsO_2^-, and the addition of two equivalents of the anion turned the color of the paper strip to dark blue. Similarly, the paper strip coated with N4R2 turned its color from yellow to green with the addition of AsO_2^-. The fabricated test strips and the color variations observed on adding arsenite are presented in Fig. 11. Similarly the test trip of N4R1 turned blue, and N4R2 and N4R3 turned cyan-green on addition of 0.5 equivalents of PO_4^{3-} as shown in Fig. S77.†

3.15.2. Solid-state sensing application. The practical application of the receptors N4R1–N4R3 for detecting arsenite is also extended in the solid state using silica gel. Silica gel (mesh size 70–230, colorless) was treated with 30% aq. Me_2SO solutions of the receptors N4R1–N4R3 and was dried in the oven to obtain the silica gel coated with the receptor. The dried silica gel coated with receptors was used to sense the arsenite anion. Two equivalents of arsenite solution were added to the treated silica gel, and an intense

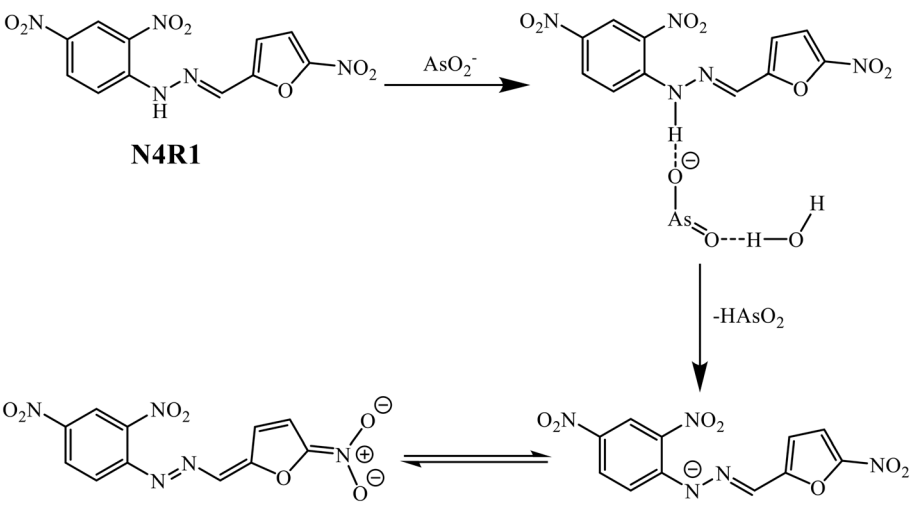

Scheme 2 The proposed detection mechanism of the AsO_2^- ion using the receptor N4R1.

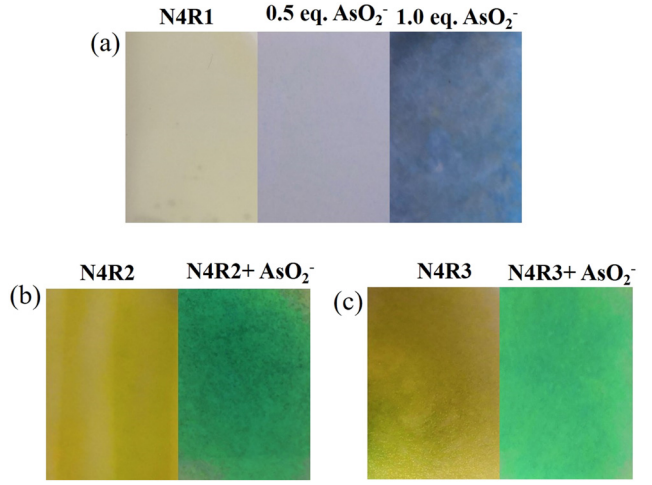

Fig. 11 Observed color changes on adding 2 equivalents of AsO_2^- ions on test strips with (a) the addition of 0.5 and 2.0 equiv. of AsO_2^- ions on test strips covered with N4R1 in 30% aq. Me_2SO, (b) N4R2 in 30% aq. Me_2SO and (c) N4R3 in 30% aq. Me_2SO.

color change was observed due to the receptor–arsenite interaction. The extra solvent was removed, and the silica gel with the receptor and the arsenite was dried in the oven. The color changes were identified, and the silica gel coated with the receptor can be used for practical applications. As shown in Fig. 12, the pale yellow-colored silica gel coated with N4R1 turned blue on adding arsenite, and N4R2 and N4R3 changed their color from pale yellow to cyan and green, respectively, with the addition of AsO_2^-.

3.15.3. Analysis of food and water samples. Various anthropogenic activities contaminate water bodies with arsenic anions and phosphates, adversely affecting the quality of crops, vegetables, and fruits. These contaminants can eventually enter the food chain. Therefore, it is imperative to assess the efficiency of the developed receptors in detecting these studied anions in both environmental water samples and food samples. To conduct this evaluation, three different water samples and four different fruit juice samples were selected and analyzed for the detection efficiency of receptors towards arsenite and phosphate ions. Different fruit and vegetable juices were freshly prepared and spiked with specific concentrations of arsenite and phosphate anions. Likewise, three distinct water samples were chosen and spiked with specified amounts of arsenite and phosphate. Efforts have been made to detect and quantify the amount of arsenite and phosphate in the samples with the receptors N4R1–N4R3. The fruits and vegetable samples like cucumber, tomato, potato, and apple were purchased from the local market in Surathkal, Karnataka, India. 5 mL juices of the samples were extracted, filtered, and diluted with distilled water to the volume of 25 mL. Similarly, water samples (tap water, river water and seawater) were collected from Mangalore area, India, and filtered for analysis without any pretreatment. The fresh samples were spiked with known amounts of AsO_2^- and analyzed using UV-vis absorption spectroscopy, and anion concentrations were calculated. A linear calibration plot between the absorbance of the receptor–anion complex and anion concentration was drawn. AsO_2^- and PO_4^{3-} ions in the spiked samples were quantitatively determined with the support of the calibration plot (Fig. S78 to S81†). The receptors display an excellent recovery for the spiked samples during the analysis with good precision. Arsenite and phosphate determination in food and water samples using N4R1 is presented in Tables 2 and 3, respectively. Tables S5 and S6, in the ESI,† present the determination of arsenite and phosphate using receptors N4R2 and N4R3.

The samples were spiked with a specific arsenite/phosphate concentration along with one equivalent of various anions like fluoride, acetate, dihydrogen phosphate, and nitrate to analyze the interference imposed by other anions. The arsenite/phosphate concentrations were calculated for these sample mixtures and tabulated in Tables S7 and S8.† The resultant data confirmed that the other anions do not cause any interference in the detection of AsO_2^- and PO_4^{3-}.

4. Conclusion

In conclusion, the study demonstrates the effectiveness of stable colorimetric sensors N4R1–N4R3 in sensitively recognizing multiple anions: arsenite, arsenate, and phosphate across a pH range of 6–12. Receptor N4R1 exhibited distinct color changes and absorption spectral shifts, enabling differentiation between arsenic anions of different oxidation states (arsenite and arsenate), as well as

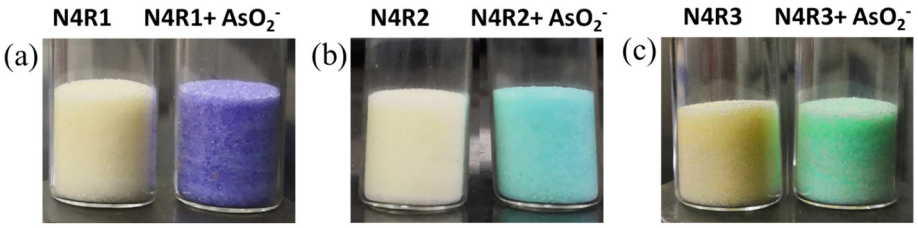

Fig. 12 Practical application of receptor (a) N4R1, (b) N4R2, and (c) N4R3 (2×10^{-5} M in 30% aq. Me_2SO) for detection of arsenite ions (1×10^{-2} M in water) by the solid silica support method.

Table 2 Determination of AsO_2^- spiked into different food and water samples using N4R1

Receptor	Samples	AsO_2^- spiked (μM)	AsO_2^- found (μM) (n = 3)	% recovery (n = 3)	% RSD
N4R1	Potato juice	2.5	2.47	98.80	0.24
	Cucumber juice	2.5	2.49	99.60	0.17
	Tomato juice	2.5	2.46	98.40	0.25
	Apple juice	2.5	2.47	98.80	0.31
N4R1	Tap water	3.0	2.99	99.66	0.08
	River water	3.0	2.97	99.00	0.17
	Seawater	3.0	2.96	98.66	0.15

RSD: relative standard deviation.

Table 3 Determination of PO_4^{3-} spiked into different food and water samples using N4R1

Receptor	Samples	PO_4^{3-} spiked (μM)	PO_4^{3-} found (μM) (n = 3)	% recovery (n = 3)	% RSD
N4R1	Potato juice	3.0	2.96	98.66	0.13
	Cucumber juice	3.0	2.99	99.66	0.25
	Tomato juice	3.0	2.96	98.66	0.17
	Apple juice	3.0	2.98	99.33	0.09
N4R1	Tap water	3.5	3.48	99.42	0.12
	River water	3.5	3.51	100.28	0.17
	Seawater	3.5	3.58	102.28	0.22

RSD: relative standard deviation.

phosphate, in a 30% aq. MeCN medium. Receptors N4R1–N4R3 identified arsenite, arsenate, and phosphate in a 30% aq. Me_2SO solution, with long-wavelength bathochromic shifts ranging from 170 to 220 nm. Additionally, ratiometric detection of the arsenite anion was demonstrated by N4R1–N4R3. ^{1}H-NMR titration and mass spectral analysis confirmed the 1 : 1 complex formation between the receptors and anions (arsenite, arsenate, and phosphate). Experimental results were validated by DFT and TD-DFT studies, and reversibility studies were conducted for arsenate and phosphates with calcium ions. The combined results from the UV-vis titration, ^{1}H-NMR titration, CV studies, mass spectral analysis, and theoretical studies suggested a hydrogen-bonding interaction between the anion and the binding site, followed by a deprotonation mechanism for the sensing process of ions by the receptors. Binding constants up to 10^6 M^{-1} and LOD in ppb levels indicate the effectiveness of the sensors for the detection of the studied multiple anions. The practical applicability of N4R1–N4R3 in detecting AsO_2^- and PO_4^{3-} was demonstrated through the fabrication of paper strips and employing silica gel for sensing. The accurate and precise detection of AsO_2^-, and PO_4^{3-} in a range of vegetable/fruit juices and environmental water samples, spiked with known quantities of anions, highlights the receptor's potential practical utility in both everyday life and environmental sample analysis. The potential interference of phosphate ions in the detection of arsenite and arsenate warrants further investigation. Future studies could focus on developing strategies to mitigate this interference, potentially through the modification of receptor structures or the optimization of detection conditions.

Author contributions

Nagaraj K: conceptualization, methodology, data curation, data analysis, writing of the original draft, visualization, and validation; A. Nityananda Shetty and Darshak R. Trivedi: supervision, formal analysis, project administration, and writing – review and editing.

Conflicts of interest

The authors declare that they have no known competing financial interests or personal relationships that could have appeared to influence the work reported in this paper. Nagaraj K, A. Nityananda Shetty, and Darshak R. Trivedi have patent on receptor N4R1 #Indian Patent No. 433799 issued to National Institute of Technology Karnataka (NITK).

Acknowledgements

NK is grateful to NITK for the research fellowship. The authors thank DST PURSE lab, Mangalore University, for ^{1}H& ^{13}C NMR analysis and CFT, NITK Surathkal, for mass analysis.

References

1 M. Šídlo, P. Lubal and P. Anzenbacher, *Chemosensors*, 2021, **9**, 1–16.
2 A. Ghosh, D. A. Jose and R. Kaushik, *Sens. Actuators, B*, 2016, **229**, 545–560.
3 U. Diwan, V. Kumar, R. K. Mishra, N. K. Rana, B. Koch, M. K. Singh and K. K. Upadhyay, *Anal. Chim. Acta*, 2016, **929**, 39–48.

4 W. C. Lin, J. W. Hu and K. Y. Chen, *Anal. Chim. Acta*, 2015, **893**, 91–100.
5 R. Chen, S. Xing, T. Hu, Y. Li, J. Chen, Q. Niu and T. Li, *Anal. Chim. Acta*, 2023, **1237**, 340557.
6 P. Ghosh and P. Banerjee, *Anal. Chim. Acta*, 2017, **965**, 111–122.
7 A. Hazra and P. Roy, *Anal. Chim. Acta*, 2022, **1193**, 339378.
8 L. Zhang, C. Wang, Y. Jiang, H. Li, H. Wang, H. Long, P. Liu, X. Xu and T. Yang, *Anal. Chim. Acta*, 2022, **1204**, 339728.
9 H. Xie, Q. Hu, X. Qin, Y. Zhang, L. Li and J. Li, *Spectrochim. Acta, Part A*, 2022, **283**, 1–6.
10 D. Wu, A. C. Sedgwick, T. Gunnlaugsson, E. U. Akkaya, J. Yoon and T. D. James, *Chem. Soc. Rev.*, 2017, **46**, 7105–7123.
11 J. Wang, J. Tong, Z. F. Wang, Q. Yuan, X. Y. Wang, S. Y. Yu and B. Z. Tang, *Anal. Chim. Acta*, 2022, **1208**, 339824.
12 J. Kim, S. Lee and M. S. Han, *Anal. Chim. Acta*, 2022, **1210**, 339879.
13 A. Mohammadi and S. Yaghoubi, *Sens. Actuators, B*, 2017, **241**, 1069–1075.
14 N. Maurya, S. Bhardwaj and A. K. Singh, *Sens. Actuators, B*, 2016, **229**, 483–491.
15 H. Singh, G. Singh, D. K. Mahajan, N. Kaur and N. Singh, *Sens. Actuators, B*, 2020, **322**, 128622.
16 B. D. Vanjare, P. G. Mahajan, H. I. Ryoo, N. C. Dige, N. G. Choi, Y. Han, S. J. Kim, C. H. Kim and K. H. Lee, *Sens. Actuators, B*, 2021, **330**, 129308.
17 P. Yin, Q. Niu, J. Liu, T. Wei, T. Hu, T. Li, X. Qin and J. Chen, *Sens. Actuators, B*, 2021, **331**, 129418.
18 J. Wang and C. S. Ha, *Analyst*, 2011, **136**, 1627–1631.
19 M. Kargar, H. R. Darabi, A. Sharifi and A. Mostashari, *Analyst*, 2020, **145**, 2319–2330.
20 L. Sun, Z. Wang, L. Chen, X. Sun, Z. Yang and W. Gu, *Analyst*, 2023, **148**, 1867–1876.
21 K. C. Chang, C. Y. Chen, C. Y. Hsu, L. W. Lee and W. S. Chung, *Analyst*, 2022, **147**, 5105–5112.
22 G. Li, L. Bai, F. Tao, A. Deng and L. Wang, *Analyst*, 2018, **143**, 5395–5403.
23 G. Men, W. Han, C. Chen, C. Liang and S. Jiang, *Analyst*, 2019, **144**, 2226–2230.
24 W.-Y. Zhu, K. Liu and X. Zhang, *Sens. Diagn.*, 2023, **2**, 665–675.
25 K. Jamuna, S. Gayathri, S. Sivakumar and B. Ashokkumar, *Sens. Diagn.*, 2023, **2**, 337–346.
26 L. K. Shaji, R. Selva Kumar, J. Jose, R. Bhaskar, V. Vetriarasu, S. G. Bhat and S. K. Ashok Kumar, *J. Photochem. Photobiol., A*, 2023, **434**, 114220.
27 A. Mujthaba Aatif, R. Selva Kumar, S. Joseph, V. Vetriarasu, S. Abdul Majeed and S. K. Ashok Kumar, *J. Photochem. Photobiol., A*, 2023, **434**, 114257.
28 S. Mishra, P. Mamidi, S. Chattopadhyay and A. K. Singh, *J. Photochem. Photobiol., A*, 2023, **434**, 114225.
29 M. Abdollahi-Moghadam, H. Keypour, R. Azadbakht and M. Koolivand, *J. Mol. Struct.*, 2023, **1273**, 134289.
30 M. Sun, X. Wang, X. Shang, X. Zhao and L. Liu, *J. Mol. Struct.*, 2022, **1250**, 131864.
31 L. Rodriǵuez-Lado, G. Sun, M. Berg, Q. Zhang, H. Xue, Q. Zheng and C. A. Johnson, *Science*, 2013, **341**, 866–868.
32 S. Paul, S. Bhuyan, S. K. Mukhopadhyay, N. C. Murmu and P. Banerjee, *ACS Sustainable Chem. Eng.*, 2019, **7**, 13687–13697.
33 N. Yogarajah and S. S. H. Tsai, *Environ. Sci.: Water Res. Technol.*, 2015, **1**, 426–447.
34 L. Chai, Y. Chen and Z. Yang, *Water Environ. Res.*, 2009, **81**, 843–848.
35 S. Dhibar, P. Yadav, T. Paul, K. Sarkar, A. P. Chattopadhyay, A. Krawczuk and B. Dey, *Dalton Trans.*, 2019, **48**, 4362–4369.
36 D. Cordell, J. O. Drangert and S. White, *Global Environ. Change*, 2009, **19**, 292–305.
37 P. J. A. Kleinman, A. N. Sharpley, R. W. McDowell, D. N. Flaten, A. R. Buda, L. Tao, L. Bergstrom and Q. Zhu, *Plant Soil*, 2011, **349**, 169–182.
38 M. S. Razzaque, *Clin. Sci.*, 2011, **120**, 91–97.
39 S. Gadiyaram, V. D. Ghule, A. Ghosh and D. A. Jose, *Sens. Diagn.*, 2022, **1**, 1224–1235.
40 M. Aatif A and S. K. A. Kumar, *J. Mol. Struct.*, 2022, **1250**, 131677.
41 K. Chauhan, P. Singh, B. Kumari and R. K. Singhal, *Anal. Methods*, 2017, **9**, 1779–1785.
42 A. K. TG, V. Tekuri, M. Mohan and D. R. Trivedi, *Sens. Actuators, B*, 2019, **284**, 271–280.
43 J. Das and P. Sarkar, *Environ. Sci.: Water Res. Technol.*, 2016, **2**, 693–704.
44 R. Purkait, S. Maity and C. Sinha, *New J. Chem.*, 2018, **42**, 6236–6246.
45 K. Chauhan, P. Singh, B. Kumari and R. K. Singhal, *Anal. Methods*, 2017, **9**, 1779–1785.
46 P. G. Sutariya, H. Soni, S. A. Gandhi and A. Pandya, *New J. Chem.*, 2019, **43**, 737–747.
47 B. Dey, R. Saha and P. Mukherjee, *Chem. Commun.*, 2013, **49**, 7064–7066.
48 T. Samanta and R. Shunmugam, *Mater. Adv.*, 2021, **2**, 64–95.
49 A. S. M. Islam, R. Alam, A. Katarkar, K. Chaudhuri and M. Ali, *Analyst*, 2015, **140**, 2979–2983.
50 A. Radujević, A. Penavic, R. Z. Pavlović, J. D. Badjić and P. Anzenbacher, *Chem*, 2022, **8**, 2228–2244.
51 A. D. Cabral, B. I. Murcar-Evans, K. Toutah, M. Bancerz, D. Rosa, K. Yuen, T. B. Radu, M. Ali, A. Penkul, D. Kraskouskaya and P. T. Gunning, *Analyst*, 2017, **142**, 3922–3933.
52 P. Kumar, S. Pachisia and R. Gupta, *Inorg. Chem. Front.*, 2021, **8**, 3587–3607.
53 M. Banerjee, S. Ta, M. Ghosh, A. Ghosh and D. Das, *ACS Omega*, 2019, **4**, 10877–10890.
54 N. Yadav and A. K. Singh, *RSC Adv.*, 2016, **6**, 100136–100144.
55 R. Purkait, S. Maity and C. Sinha, *New J. Chem.*, 2018, **42**, 6236–6246.
56 L. Zhang, X. R. Chen, S. H. Wen, R. P. Liang and J. D. Qiu, *TrAC, Trends Anal. Chem.*, 2019, **118**, 869–879.
57 A. Singh and D. R. Trivedi, *AIP Conf. Proc.*, 2019, **2142**, 1–6.
58 K. Nagaraj, A. N. Shetty and D. R. Trivedi, *Indian Pat.*, 433799, 2023.
59 K. Nagaraj, A. N. Shetty and D. R. Trivedi, *Anal. Chim. Acta*, 2023, **1265**, 341355.

60 Madhuprasad, N. Swathi, J. R. Manjunatha, U. K. Das, A. N. Shetty and D. R. Trivedi, *New J. Chem.*, 2014, **38**, 1484–1492.
61 V. Tekuri, S. K. Sahoo and D. R. Trivedi, *Spectrochim. Acta, Part A*, 2019, **218**, 19–26.
62 S. Pangannaya, M. Mohan and D. R. Trivedi, *New J. Chem.*, 2018, **42**, 10406–10413.
63 K. S. Keremane, R. Rao and A. V. Adhikari, *Photochem. Photobiol.*, 2021, **97**, 289–300.